Numerical Modeling of an Underwater Vehicle

Mech 499 Final Report

Dean Steinke
April 26, 2003

Supervisor: Brad Buckham

Summary

This Mech 499 report summarizes the development of a numerical AUV model that coupled an appropriate thruster model with an approximate underwater vehicle model. The model was created to promote an understanding of the dynamics of underwater vehicles and create a useful design tool for AUVic. The governing dynamics of underwater vehicles are reviewed. The hydrodynamic forces on the vehicle are considered. For the numerical vehicle model, estimates of the added mass and inertia are found using a strip theory technique. The translational drag of the vehicle is estimated using available empirically determined drag coefficients. Drag coefficients for the rotational motion of the vehicle are estimated using available 2D translational coefficients. A four quadrant thruster model is reviewed that combines an armature controlled motor model, a theoretical propeller mapping using airfoil theory, and a fluid momentum model. Finally, a program that was used to numerically model the ARCS vehicle, and was modified to represent the AUViking vehicle, is reviewed. This paper discusses how the thruster model was adapted to represent AUViking's thrusters and how estimates of the hydrodynamic forces were incorporated into the numerical model. Several simulations are reviewed in this report.

Table of Contents

Introduction

A group of engineering and computer science students from the University of Victoria are working to build an Autonomous Underwater Vehicle (AUV). The group is called AUVic, and the AUV has been named AUViking (www.engr.uvic.ca/~auv). The AUV is being designed to compete in the 6th International AUV Competition hosted by the Association for Unmanned Vehicles Systems International (www.auvsi.org). Little was known about the issues surrounding the construction of an AUV. As a result, a numerical model of the AUV has been created as part of a Mech 499 project. The scope of the work is summarized in this report.

The numerical model was created to help the design of the AUViking and promote an understanding of the dynamics of underwater vehicles. The design of AUViking is well underway. A picture of the solid model is presented in Figure 1. It is principally made up of an upper polycarbonate shell, and a lower UHMW plate. A vertical thruster runs through the center of vehicle shell. The principle dimensions of the vehicle are 17.5"x23.5"x6". The electronics and batteries are contained underneath the shell.

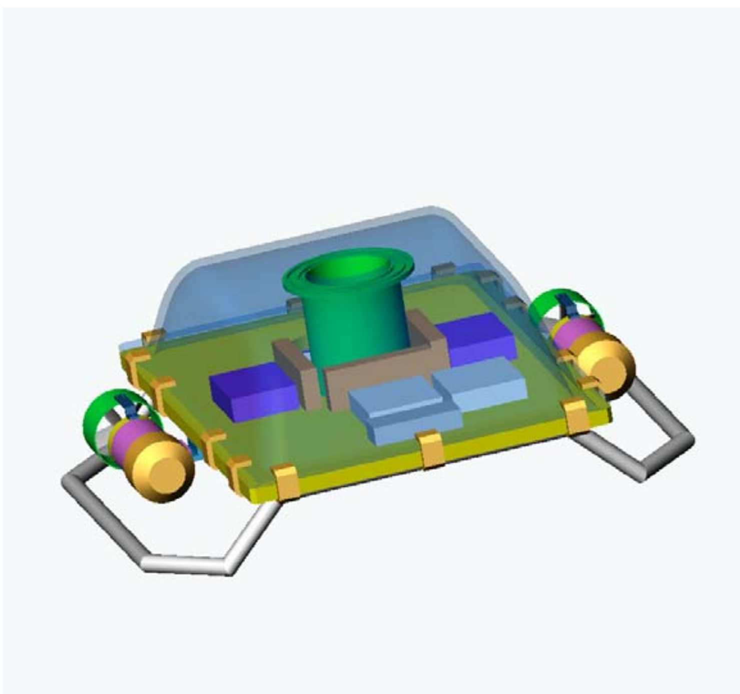

Figure 1 3D model of AUViking

The modeling and control of underwater vehicles is difficult. The governing dynamics of underwater vehicles are fairly well understood, but they are difficult to handle for practical design purposes. The problem includes many nonlinearities and modeling uncertainties. It was the aim of this 499 project to couple an appropriate thruster model with an approximate underwater vehicle model. Many hydrodynamic and inertial nonlinearities are present due to coupling between degrees of freedom [1]. The presence of these non-linear terms requires the use of a numerical technique to determine the vehicle response to thruster inputs and external disturbances over the wide range of operating conditions.

The report outlines the creation of the numerical model for the AUViking. First, how the dynamic model of an underwater vehicle is implemented is reviewed. The hydrodynamics of the vehicle are discussed (this includes a discussion on the calculation of drag and added mass terms). Second, the thruster model developed by Healey et al. [2] is reviewed. How the thruster dynamics and four quadrant mapping is coded and integrated into the vehicle model is also analyzed. Fourth, there is a review of how the thruster model parameters presented by Healey et al. were adapted to approximate the thrusters being built by AUVic. Fifth, an outline of the entire AUViking simulation program is presented. Lastly, the results of 3 simulations are considered: a dive, a forward surge, and a turn.

Vehicle Dynamics

The vehicle is a free-body in space with mass and inertia, being acted on by numerous forces (see Figure 2). Using Newton’s second law the motion of the vehicle can be defined by

$$\sum \vec{F} = \underline{\underline{M}}\vec{a}_I \tag{1}$$

$$\sum \vec{M} = \underline{\underline{I}}\vec{\alpha}_I + \omega_I \times \underline{\underline{I}}\omega_I \tag{2}$$

where $\underline{\underline{I}}$ and $\underline{\underline{M}}$ are inertial and mass matrices respectively. In the numerical model for the vehicle we evaluate 1 and 2 to find the linear and angular accelerations, $\vec{a}$ and $\vec{\alpha}$ respectively. Augmenting these accelerations with the vehicle’s velocities, the vehicle state can be integrated using a numerical integration technique to find the vehicle’s velocity, orientation and position at the next state.

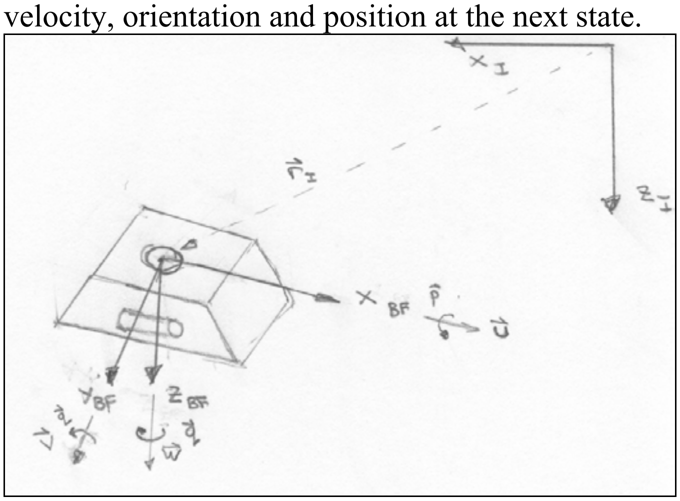

Figure 2 Frame Assignments

It is difficult to specify the vehicle parameters $\underline{\underline{I}}$ and $\underline{\underline{M}}$ in an inertial or earth fixed frame, since as the body moves these parameters would change. When a reference frame is attached to the vehicle, the parameters $\underline{\underline{I}}$ and $\underline{\underline{M}}$ are constant with respect to the moving axis (Figure 2 shows how the inertial and body fixed frames are assigned). So, in the numerical model for the vehicle we want to evaluate (1) and (2) to find the linear and angular accelerations in the body fixed frame ($\vec{a}_{BF}$ and $\vec{\alpha}_{BF}$). The difficulty is that when (1) and (2) are evaluated in the body fixed frame, we don't know about the position, orientation or velocity of the vehicle with respect to an inertial frame. To get around this problem, the vehicle orientation is represented using a set of Bryant angles.

The Bryant angles are a set of angles that define 3 rotations which bring the inertial frame into alignment with the body frame. Bryant angles which determine the orientation of the body frame are be labeled as

$$\beta = \begin{bmatrix} \phi \\ \theta \\ \psi \end{bmatrix} \tag{3}$$

The first rotation ψ is about the Z axis of the inertial frame (yaw). The second rotation θ is about the new Y axis (pitch). The last rotation, φ, is about the new X axis (roll). The resulting transformation matrix $\underline{\underline{R}}$ can be defined as [2]

$$\underline{\underline{R}} = \begin{bmatrix} c\theta c\psi & s\phi s\theta c\psi - c\phi s\psi & c\phi s\theta c\psi + s\phi s\psi \\ c\theta s\psi & s\phi s\theta s\psi + c\phi c\psi & c\phi s\theta c\psi + s\phi c\psi \\ -s\theta & s\phi c\theta & c\phi c\theta \end{bmatrix} \tag{4}$$

The translational velocities in body fixed frame can be found by

$$\vec{v}_I = \underline{\underline{R}}\vec{v}_{BF} = \begin{bmatrix} c\theta c\psi & s\phi s\theta c\psi - c\phi s\psi & c\phi s\theta c\psi + s\phi s\psi \\ c\theta s\psi & s\phi s\theta s\psi + c\phi c\psi & c\phi s\theta c\psi + s\phi c\psi \\ -s\theta & s\phi c\theta & c\phi c\theta \end{bmatrix} \begin{bmatrix} u \\ v \\ w \end{bmatrix} \tag{5}$$

Also, if the rotational velocities are known in the body fixed frame (p, q, r in Figure 2) and the set of Euler angles is known, it can be shown that the rates of change in Euler angle rates can be determined by

$$\dot{\beta} = \underline{\underline{T}}\vec{\omega}_{BF} = \begin{bmatrix} \dot{\phi} \\ \dot{\theta} \\ \dot{\psi} \end{bmatrix} = \begin{bmatrix} 1 & s\phi t\theta & c\phi t\theta \\ 0 & c\phi & -s\phi \\ 0 & \frac{s\phi}{c\theta} & \frac{c\phi}{c\theta} \end{bmatrix} \begin{bmatrix} p \\ q \\ r \end{bmatrix} \tag{6}$$

where $\dot{\beta} = \frac{d}{dt}\beta$.

As mentioned earlier, in the numerical model for the vehicle we evaluate (1) and (2) to find the linear and angular rates of change in the body fixed frame ($\vec{a}_{BF}$ and $\vec{\alpha}_{BF}$). Before these terms are integrated we need relate them to the inertial frame. This is done by differentiating (6) and applying (4) to the body-fixed acceleration

$$\vec{a}_I = \dot{\underline{\underline{R}}}\vec{v}_{BF} + \underline{\underline{R}}\vec{a}_{BF} \tag{7}$$

$$\ddot{\beta} = \dot{\underline{\underline{T}}}\vec{\omega}_{BF} + \underline{\underline{T}}\vec{\alpha}_{BF} \tag{8}$$

The steps followed in the dynamic model are summarized in Figure 3.

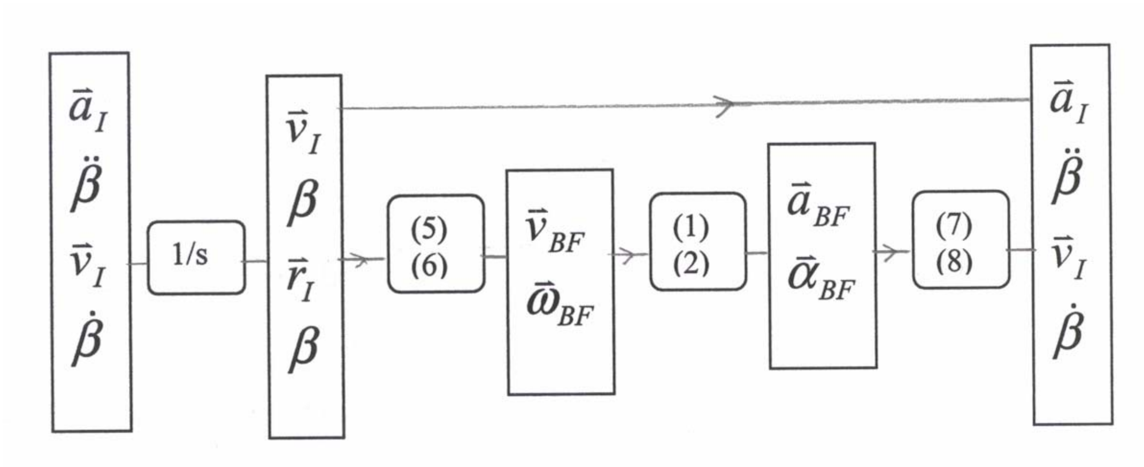

Figure 3 Flow Chart of Vehicle Dynamic Model

The next step in the modeling of an underwater vehicle is to come up with estimates of the parameters that govern the hydrodynamic and gravitational loadings. Once these are defined the forces acting on the vehicle are determined. The forces acting on the vehicle can be divided into hydrodynamic and control forces. For this project the hydrodynamic forces were estimated using empirically based coefficients. The thrusters are the only control forces on AUViking. The thruster forces were determined using a dynamic thruster model.

Vehicle Parameters

AUViking's general layout can be seen in Figure 4. A horizontal thruster is located on the both the port and starboard sides of the vehicle. A vertical thruster pushes the vehicle down through the water.

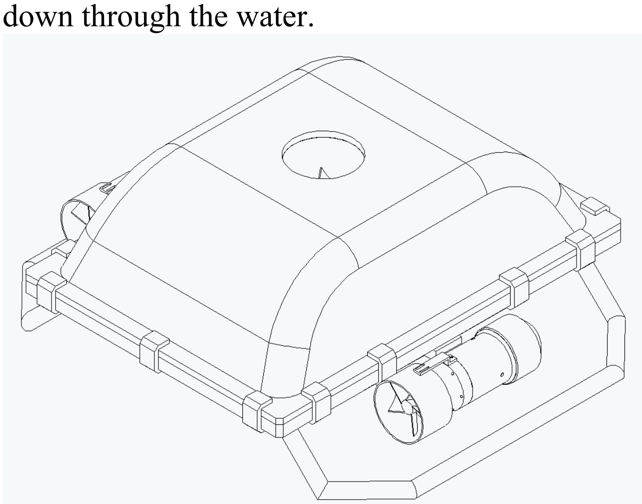

Figure 4 ISO View of AUViking

Figure 5 and Figure 6 show the front and side views of AUViking, respectively. These figures also the principle dimensions of the polycarbonate hull. The vehicle will weigh approximately 32 kg when finished. The vehicle design is intended to allow for slow and precise maneuvering. It is designed for relatively short missions; most missions that it will be executing will be around 20 minutes long.

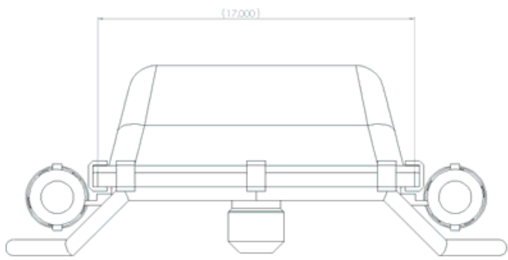

Figure 5 Front View AUViking

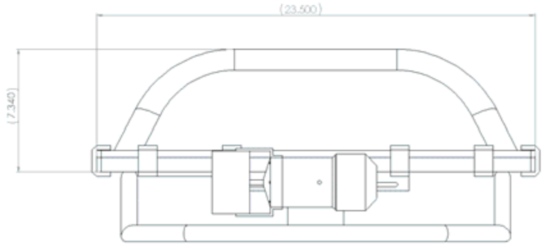

Figure 6 Side View AUViking

The vehicle model shown in Figure 4 Figure 6 was created using 3D modeling software. The vehicle's moments and products of inertia were determined from the 3D model of the vehicle.

Hydrodynamic Forces

Added Mass

When the body is accelerated, the surrounding fluid is also accelerated. The body is essentially pushing an extra mass which gives rise to a force that opposes the acceleration of the vehicle. This phenomenon is called *added mass*.

The challenge is to realistically estimate the effect of added mass on the vehicle dynamics. According to potential theory the added mass depends only on the shape and direction of motion [1]. Fossen [5] showed how the fluid's kinetic energy can be used with Kirchoff's equations to find expressions for the forces and moments that act on the body. The approach is valid if the fluid is assumed to be irrotational and inviscid. He showed that the added mass forces are non-linear and are dependent on the vehicle motion. Fossen's approach is summarized as

$$\vec{F}_A = \underline{\underline{M}}_A \dot{\vec{v}} + \underline{\underline{C}}_A(\vec{v})\vec{v} \qquad (9)$$

where $\underline{\underline{M}}_A$ is the added mass matrix and $\underline{\underline{C}}_A$ Coriolis added mass matrix. The terms in the 6x6 added mass matrix $\underline{\underline{M}}_A$ are called hydrodynamic derivatives, and have the units of mass. $\underline{\underline{M}}_A$ is defined as:

$$\underline{\underline{M}}_A = \begin{bmatrix} x_{\dot{u}} & x_{\dot{v}} & x_{\dot{w}} & x_{\dot{p}} & x_{\dot{q}} & x_{\dot{r}} \\ y_{\dot{u}} & y_{\dot{v}} & y_{\dot{w}} & y_{\dot{p}} & y_{\dot{q}} & y_{\dot{r}} \\ z_{\dot{u}} & z_{\dot{v}} & z_{\dot{w}} & z_{\dot{p}} & z_{\dot{q}} & z_{\dot{r}} \\ l_{\dot{u}} & l_{\dot{v}} & l_{\dot{w}} & l_{\dot{p}} & l_{\dot{q}} & l_{\dot{r}} \\ m_{\dot{u}} & m_{\dot{v}} & m_{\dot{w}} & m_{\dot{p}} & m_{\dot{q}} & m_{\dot{r}} \\ n_{\dot{u}} & n_{v} & n_{\dot{w}} & n_{\dot{p}} & n_{\dot{q}} & n_{\dot{r}} \end{bmatrix} \tag{10}$$

The first entry is defined as

$$x_{\dot{u}} = \frac{\partial F_{Ax}}{\partial \dot{u}} \tag{11}$$

where F_{Ax} is a hydrodynamic force in the x direction. The other entries are similarly defined by partial derivatives of the added mass force with respect to accelerations. The Coriolis added mass matrix $\underline{\underline{C}}_A$ is made up of velocity components in the local frame and hydrodynamic derivative terms.

Examining (9) it can be seen that the force is dependent both on vehicle velocity and acceleration. But by noting that in many underwater vehicle applications the vehicle moves slowly and has many planes of symmetry the effects of the off diagonal terms in the added mass matrix can be neglected. This means that the added mass effect in each direction is not dependent on the vehicle motion in the other directions. The Coriolis matrix is simplified by this assumption as well. In addition, the Coriolis terms are second order velocity terms, so if the velocities are low these terms can be neglected. AUViking will be moving at relatively slow speeds so the Coriolis terms should be reasonably neglected. Caccia et al. [4] neglected the Coriolis kinematics and achieved acceptable results. The diagonal terms of the added mass matrix are still to be determined.

The remaining hydrodynamic derivatives can be determined empirically or theoretically. The empirical method would involve testing the vehicle. Caccia et al. put forward a process for determining the added mass effects and the drag on the vehicle. Their method involves testing each degree of freedom independently. This will not be possible because the vehicle which the model that is being developed for has not yet been built. Doing this would be relatively cheep, but it is really too late for practical design purposes. One of motivating factors for modeling the vehicle was to help establish a design. If the vehicle is already constructed, then revisions may be difficult or impossible.

Theoretically, the hydrodynamic derivatives can be determined using an approach called strip theory. Fossen provides some two-dimensional added mass coefficients [5]. If the vehicle is divided into a number of strips, the added mass for each 2D strip can be computed and summarized over the length of the body to get the 3D hydrodynamic derivative. This is how the added mass terms were computed for the AUViking simulation. A box with the principle dimensions was taken to represent the hull. The origin set at the center of gravity of the box. Fossen showed that the 2D mass coefficient in the $\dot{u}$ direction is written as

$$x_{\dot{u}} = -\int_{-W/2}^{W/2} A_{11}^{(2D)} dy \qquad (12)$$

- A_{11} is the hydrodynamic derivative in the first position of the added mass matrix. In this case the cross-sectional shape of the hull parallel to the flow in the x-direction is a rectangle (shown by the shaded strip in Figure 7). $A_{11}^{(2D)}$ for this cross-section is found using the graph in Figure 8 [5], the dimensions L and H and the density of water. Now 12 can be integrated to find $x_{\dot{u}}$. The same procedure is followed for $y_{\dot{v}}$ and $z_{\dot{w}}$.

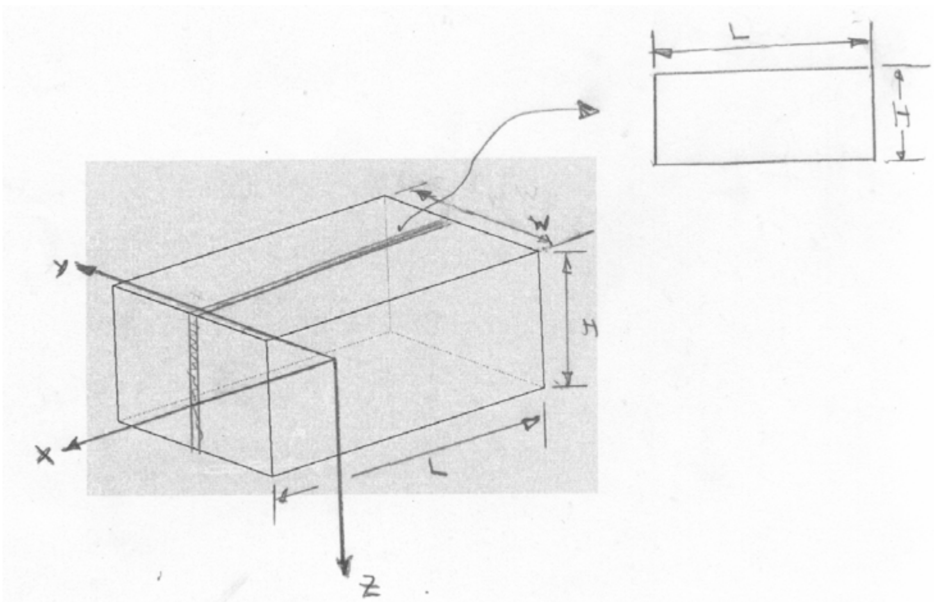

Figure 7 Integration of 2D added mass coefficients

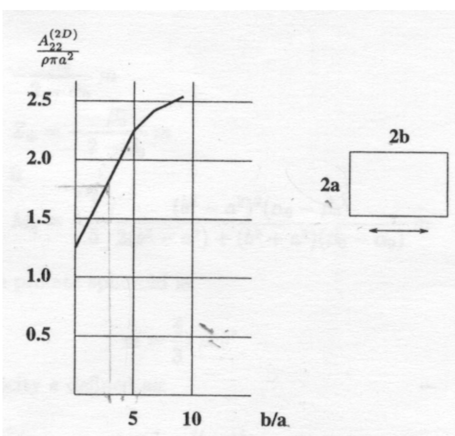

Figure 8 2D added mass for a rectangular cross-section [5]

Determination of the surge direction added mass would work as follows:

$\rho := 1000 \frac{kg}{m^3}$ W := 17.5·in H := 5.75·in

$\frac{L}{H} = 4.087$

F := 2.0 *F = Rectangular cross section 2D coefficient from Figure 8*

$$A_{11} := F \cdot \rho \cdot \pi \cdot \left(\frac{H}{2}\right)^2 2 \cdot \frac{W}{2}$$ *- Integrating equation (12)*

$$A_{11} = 14.893 \cdot kg$$

Fossen showed that the determination of the two-dimensional added moment of inertia in roll can be written as [5]:

$$-l_{\dot{p}} = \int_{-L/2}^{L/2} A_{44}^{(2D)} dx = \int_{-W/2}^{W/2} y^2 A_{33}^{(2D)} dy + \int_{-H/2}^{H/2} z^2 A_{22}^{(2D)} dz \qquad (13)$$

Equation 13 shows that translational 2D added mass coefficients can be used to find the added inertia in the roll direction. Equation 13 is found by applying the parallel axis theorem to each individual strip. Expressions similar to 13 for finding the added inertia in pitch and yaw ($m_{\dot{q}}, n_{\dot{r}}$) can be found in Fossen [5].

Translational Drag

The hydrodynamic drag and lift forces depend on the shape of a hull. Typically, determination of the hydrodynamic characteristics of a vehicle is determined experimentally in expensive tow tank tests. Caccia et al. improved on this by using on board sensors to determine drag coefficients for each of the degrees of freedom independently. This could not be done for our case, because the vehicle isn't built yet. However, the use of available empirically determined drag coefficients for common shapes to estimate the drag forces is possible. The use of these terms assume that the total drag in each direction is independent of drag in other directions.

Drag force is dependent on vehicle velocity and geometry; a drag coefficient C_D contains this information. The surge direction the drag force is defined as

$$F_H^x = -\frac{1}{2} \rho A^x C_D^x u|u| \qquad (14)$$

Equation 14 can be used to find the drag force in the y and z direction as well. This force always acts in opposition to the motion of the vehicle. Because of the stubby shape of the AUV, the drag coefficients for the translational directions can be estimated to be similar to the empirically determined drag coefficients for a cube or rectangular plate. For the AUViking simulation, the shape of the hull was estimated to be a cube. Using data from White [6] the coefficient of drag was estimated to be 1.07 for each direction. The characteristic area is taken as the area of the face perpendicular to the flow.

In the model the drag forces were implemented at the center of pressure of each of the faces perpendicular to the flow. This assumption would work well if the AUV was actually a box. But the curved upper surface of the vehicle does not have clear center of pressure at which to apply the drag force. The direction that the force is applied is also not certain. What this model does provide is coupling between degrees of freedom. This is something that the Caccia model did not do [3]. For instance, the foreplane center of pressure is located above the center of gravity. Thus, when the vehicle moves forward the drag force will cause the vehicle to pitch. By varying the location of the point at which the drag force is applied one can get an idea of the stability of vehicle design. Say, if there is no appreciable change in pitch angle as the drag force application point location is varied then - the vehicle design is probably reasonably "stable". But if varying the center of pressure causes the vehicle to change its pitch orientation greatly – the design is most likely not optimal.

Rotational Drag

Drag coefficients for the rotational motion of the vehicle are not readily available. It is proposed that the translational coefficients be determined from available drag coefficients. This was done by first considering that in rotational motion the velocity increases as you move from the axis of rotation. Half of the object can be broken into small strips - starting at the central axis and moving outward (see Figure 10). Each strip has its own velocity. The drag force for each strip can be determined by selecting an appropriate 2D drag coefficient from White [15] and finding the translational velocity of strip. Then the force can be expressed as a moment by multiplying the strip by its position relative to the central axis. Figure 9 shows how this can be done.

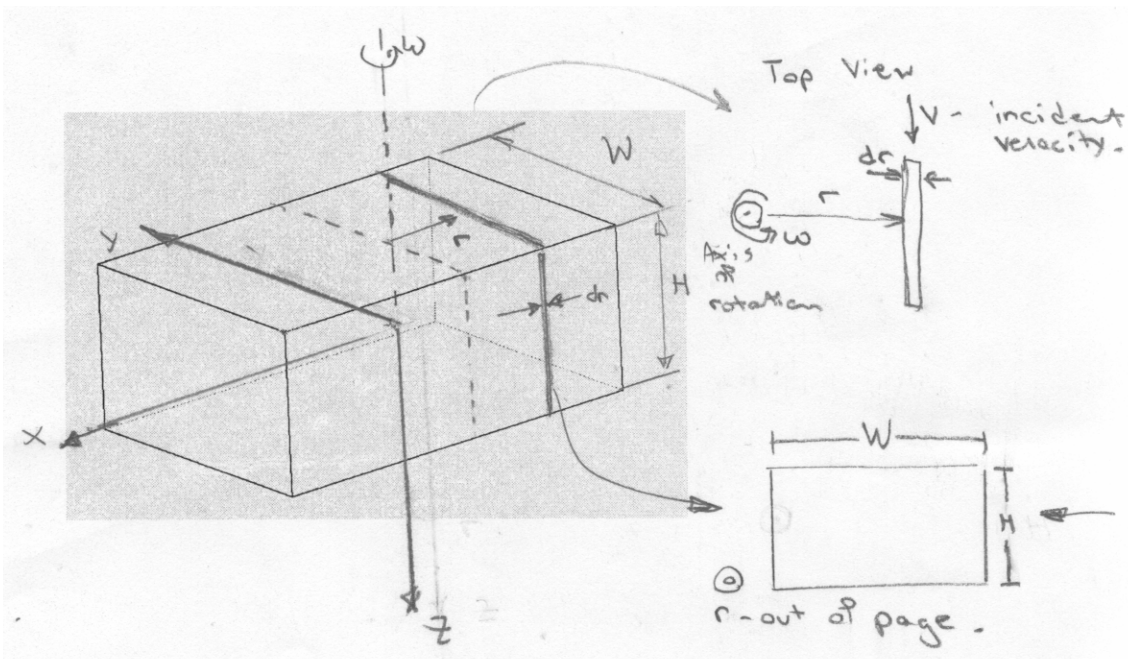

Figure 9 Drag on vehicle due to rotation

In order to implement the idea presented above to the AUViking model some estimations were made. If one looks at the top view of the rotating cube it can be seen that the drag forces in rotational motion could be assumed to act principally on 4 half faces of the cube (Figure 10). The drag forces are create the resulting moment about the axis of rotation. To determine the overall moment, the block is divided into strips. To make the computation of the moment due to drag easier, it is estimated that velocity over each strip is constant and is equal to the rotational rate times the distance to the strip. If the drag forces acting on these small strips are added up through integration, the total moment exerted about the axis of rotation can be determined.

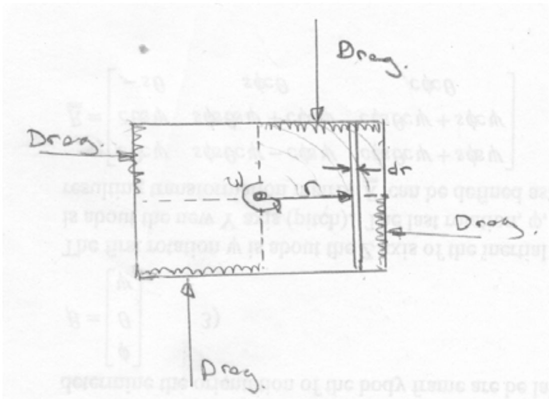

Figure 10 Top view of rotating cube

If the coefficient of drag C_D, the water density and height H is constant for the whole integration, the moment acting on half of the object will be

$$M_H^i = \int_0^r r dF_{strip} = \frac{1}{2} C_D^i H \rho \omega^{i^2} \int_0^r r^3 dr = \frac{1}{2} C_D^i H \rho \omega^{i^2} \frac{r^4}{4} \qquad (15)$$

The coefficient of drag for each characteristic shape was found by interpolating the data in the Figure 11.

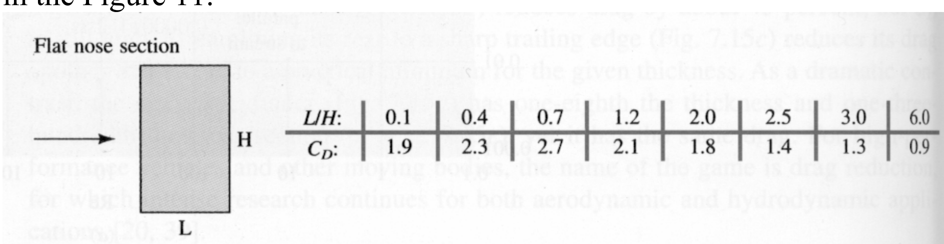

Figure 11 2D Drag coefficients

For example, for the drag induced moment about the x-axis two drag coefficients were found using the table in Figure 11:

$$\frac{H}{L} = 0.245$$

$$CDL_1 := \left(\frac{1.9 - 2.3}{.1 - .4}\right) \cdot \left(\frac{H}{L} - .1\right) + 1.9$$

$$CDL_1 = 2.093$$

$$\frac{W}{L} = 0.745$$

$$CDL_2 := \left(\frac{2.7 - 2.1}{.7 - 1.2}\right) \cdot \left(\frac{W}{L} - .7\right) + 2.7$$

$$CDL_2 = 2.646$$

If the body is symmetric about the axis of rotation the result of (15) can be multiplied by two – otherwise the procedure can be repeated for the other half of the object. The moment computed with equation 15 is an estimation of the moment due to the drag force on one face of the cube in Figure 10. This procedure may not be a very good one.

Control Forces (Thruster Model)

Figure 12 shows the schematic of a typical thruster. V is the vehicle velocity, V_a is the velocity of the fluid through the shroud, and T is the output thrust on the vehicle. There is a good history of research on ship propellers but much of this research isn't applicable to underwater vehicles. Underwater vehicles move relatively quickly and often execute a full range of positioning maneuvers. The time scale of the flow dynamics though underwater vehicle thrusters is generally much smaller than that of large ship propellers [6]. Underwater vehicle thrusters also operate in conditions not normally experienced by ship propellers. Traditional propeller theory related the thrust output directly to shaft torque. Traditionally only steady conditions were generally considered. But for underwater vehicles, where precise control is necessary, a more accurate dynamic model is necessary.

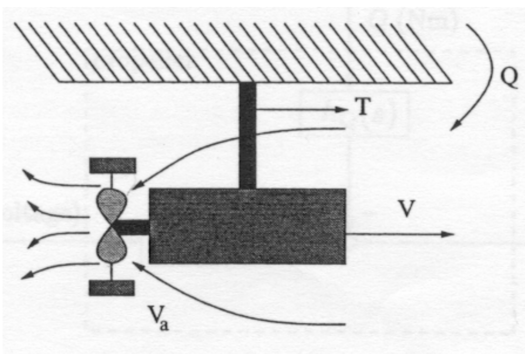

Figure 12 Schematic of a typical thruster

Yoerger et al. [6] developed a dynamic thruster model for use in underwater vehicles. The propeller angular velocity Ω was used as the dynamic variable. The thrust output was determined to be

$$F_{thrust} = C_t \Omega^2 \tag{16}$$

where C_t is a constant depending on physical thruster parameters. This model was an improvement over previous ones because it related the propeller angular velocity to shaft the shaft torque τ by

$$\dot{\Omega} = \beta\tau - \alpha\Omega^2 \tag{17}$$

where β and α are constants depending on physical thruster parameters. This model took the fluid momentum in the shrouding area into consideration. This introduced a time lag in the model that more accurately represented the delay between motor control signals and developed thrust.

Yoerger's model only considered the case when the velocity of the fluid through the shroud is positive (as shown in Figure 12) and the prop rotational rate was in the direction that would produce a positive flow. But other combinations of prop rotational rate and flow direction (V_a) are possible. The idea of four quadrant operation of thrusters was developed by Van Lammeren et al. [7] when accurate ship maneuvering models were desired. The four quadrants are characterized by the four different possible combinations of propeller rotation rate and flow velocity through the thruster. Yoerger's model only considered operation in the quadrant defined by positive propeller rotational rate and positive flow velocity through the thruster.

The model developed by Van Lammeren characterized propellers in terms of nondimensionalized coefficients of propeller thrust and torque as a function of the apparent angle of approach of water particles on the blades. The four-quadrant data were fitted with Fourier series of 10 and 20 terms so that props could be numerically represented as part of a simulation model. These terms are determined from experimental data and are unique for each prop. Healey et al. [2] developed a four quadrant model that was easier to apply. Healey's model was used to simulate AUViking's thrusters. Healey's model will be looked at next. Healey's model combines an armature controlled motor model, a theoretical propeller mapping using airfoil theory and a fluid momentum model applied within the finite volume of the shrouded region.

Motor Modeling

In Healey's model, the control signal to the thruster is voltage. The motor dynamics are governed by the torque load on the shaft τ_L, the propeller rotational rate Ω, and the applied voltage V_a. Considering only the motor dynamics, the rotational rate of the motor is governed by

$$\dot{\Omega} = -K_1\Omega + K_2V_a - K_h\tau_L \qquad (18)$$

K_1 relates the motor shaft acceleration to the back emf developed in the motor. It is assumed to be linear and is defined as

$$K_1 \cong \frac{K_bK_m}{R_aJ} \qquad (19)$$

K_b, K_m and R_a are motor constants that are generally provided with most motors. K_b is the back-emf constant. K_m is the motor toque constant. R_a is the armature resistance. J is the inertia of the armature, shaft, and propeller.

In (18), K_2 relates the motor torque to the current or voltage applied to the motor. It is defined as

$$K_2 = \frac{K_m}{R_aJ} \qquad (20)$$

K_h relates the effect of the load (torque) on the motor acceleration. Healey approximates this as the inverse of the motor shaft inertia. The inertia of the motor shaft is provided with the motor data. For the AUViking simulation the inertia of the prop was found using 3D modeling software.

$$K_h \approx \frac{1}{J} \qquad (21)$$

The motors that are going to be used in AUViking's thrusters are 77 Watt, 12V Globe-Motors. These are similar to the motors used by Healey. The values for K_1, K_2 and K_h for Healey's motors model and AUVikings are provided in the table below.

Table 1 Motor Parameters

	AUViking's 12V Globe-Motors	Healey's 24V Pittman Motors
K_1	32.34	70.15
K_2	1107.5	1133.2
K_h	18900	17790

Propeller Mapping

The propeller mapping proposed by Healey involves applying airfoil theory to the propeller to find the thrust and torque on the propeller. Treating the prop blade as an airfoil involves estimating the direction of the incoming fluid particles on the blade, so that the lift and drag on the airfoil can be estimated. The direction of the incoming particles is measured by the effective angle of attack α_e, which is the angle between the velocity of incoming particles and the chord line of air foil. The four quadrants of operation will be defined by the angle of attack. Figure 13 shows how the effective angle of attack is defined.

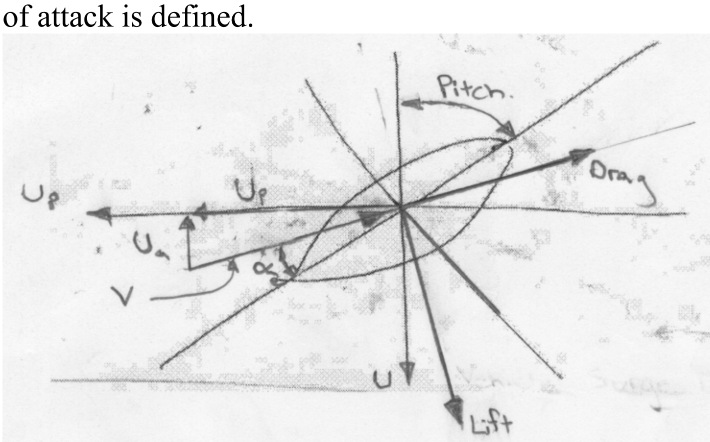

Figure 13 Angle of attack diagram for propellor blade (Quadrant 1 of the four quadrant map)

V is the velocity incoming fluid particles on the prop, and it is dependent on U_a and U_p. U_a is the velocity of fluid passing through the propeller shroud. U_p is the velocity of the propeller blade, defined as

$$U_p = .7R\Omega \qquad (22)$$

R is the radius of the prop. The '.7' in equation 22 refers to the location of the blade center of pressure. Ω is the prop rotational rate. It is known that a lift force will be developed on the prop perpendicular to the line of action of the incoming flow V. This line of action is defined by the effective angle of attack, α_e. Similarly, a drag force will develop in line with the flow. Resolving the lift and drag forces into the vehicle direction

U and the propeller direction U_p, will yield the thrust and torque developed by the prop. The four quadrants of operation of the propeller are defined by the direction of the velocity V. Figure 13 shows the 1st quadrant of operation (U_a>0, U_p>0). Figures 14, 15 and 16 show the other possible quadrants of operation (different combinations of U_a and U_p). Figures 14, 15 and 16 also show the lift and drag forces that are developed by the fluid flow. The lift and drag forces are dependent on the fluid velocity and the effective angle of attack α_e.

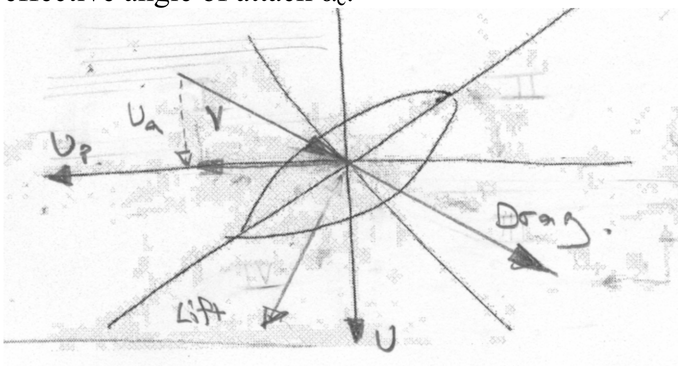

Figure 14 Four quadrant mapping, Quadrant 2

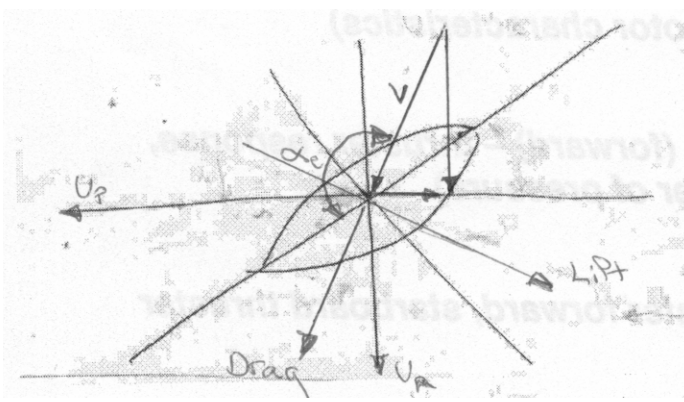

Figure 15 Four quadrant mapping, Quadrant 3

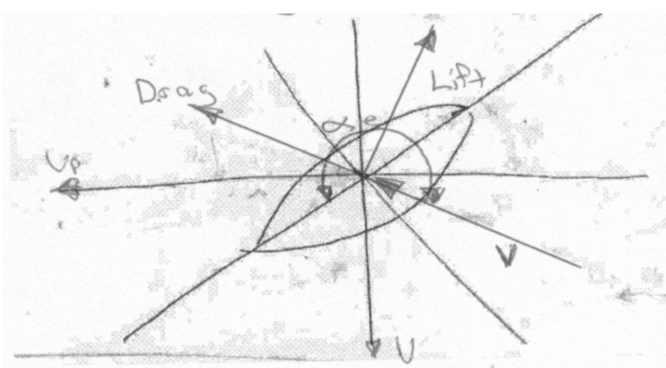

Figure 16 Four quadrant mapping, Quadrant 4

Healey et al. proposed that the lift and drag coefficients be determined from simple harmonic functions of the angle of attack (see Figure 17). Only the maximum coefficients of lift and drag, and the angle of attack are needed to find the lift and drag coefficients.

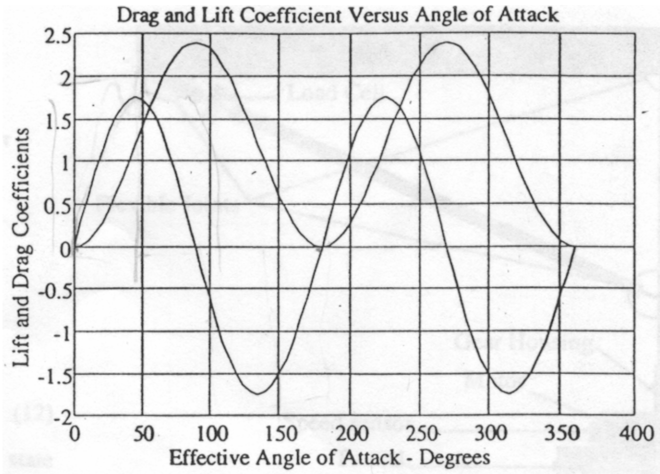

Figure 17 Proposed lift and drag force coeficients versus angle of attack [2]

It can be seen from Figure 17 that the effective angle of attack must be known for all quadrants of operation (0 - 2π). It was determined that in quadrants 1 and 2 α_e is calculated by

$$\alpha_e = \left(\frac{\pi}{2} - p\right) - \arctan\left(\frac{U_a}{U_p}\right) \tag{23}$$

where p is the pitch. In quadrants 3 and 4 the angle of attack is determined using

$$\alpha_e = \left(\frac{3\pi}{2} - p\right) - \arctan\left(\frac{U_a}{U_p}\right) \tag{24}$$

In the simulation, determining which equation to use is done by checking the sign of Ω. Using the angle of attack calculated in (23) and (24) the lift and drag forces are now

$$Lift = 0.5\rho V^2 A C_{L\max} \sin(2\alpha_e) \tag{25}$$

$$Drag = 0.5\rho V^2 A C_{D\max} (1 - \cos(2\alpha_e)) \tag{26}$$

To find thrust and torque on the motor the lift and drag forces need to be resolved. Resolving the forces into the thrust and torque was done by determining that the angle between the line of action of lift and the U axis. This angle was determined for all four quadrants to be

$$\theta = \frac{\pi}{2} - p - \alpha_e \tag{27}$$

Then, by defining the rotation matrix

$$R_\theta = \begin{bmatrix} \cos\theta & -\sin\theta \\ \sin\theta & \cos\theta \end{bmatrix} \tag{28}$$

the output thrust and force on the prop can be determined by

$$\begin{bmatrix} T \\ F_P \end{bmatrix} = R_\theta \begin{bmatrix} Lift \\ Drag \end{bmatrix} \tag{29}$$

The torque load on the motor can be found using

$$\tau_{L:} = 0.7 R F_P \tag{30}$$

Equation 30 can be used in the propeller dynamic equation (18). Now that thrust and torque loading, the effect of fluid dynamics on the thruster model is considered.

Fluid Modeling

Healey et al. connected the motor model and the propeller maps by applying the momentum equation to a control volume surrounding the inlet flow. This couples the rotational rate of the motor Ω to the velocity of the flow through the shroud, U_a. The flow velocity is governed by

$$\dot{U}_a = -K_4 K_3^{-1} \overline{U}_a \left|\overline{U}_a\right| + K_3^{-1} T \tag{31}$$

where

$$K_3 = \rho A L \gamma \tag{32}$$

and

$$K_4 = \rho A \Delta\beta \tag{33}$$

and

$$\overline{U}_a = U_a - U \tag{34}$$

where U is the vehicle velocity at the thruster. γ and $\Delta\beta$ are experimentally determined coefficients. For the AUViking model γ and $\Delta\beta$ were taken from the Healey test case. The propellers Healey used are of similar pitch (45º) and diameter (3”) to the ones used on the AUViking.

By knowing how the rotation rate of the motor is changing (18), and how the flow rate through the propeller is changing (31) – the thrust at a later time may be determined by integrating these equations forward. Since thrust is a function of Ω and U_a.

Vehicle Simulation

The code used to numerically model AUViking was originally written to model the ARCS vehicle. MatLab® is used for the simulation. The data was modified to represent AUViking for this project. Figure 18 shows the program layout. *AUVikingsim.m* is the main program. It loads the vehicle, motor and thruster parameters then runs the MatLab® numerical integration function *ode45*. *ode45* calls *AUVikingdyn.m* which returns the derivatives of the state vector quantities. *thruserdyn.m* analyzes the thruster dynamics, while *AUVikingdyn.m* evaluates the overall vehicle dynamics. The state vector for the simulation is:

$$X = \begin{bmatrix} v_I^x \\ v_I^y \\ v_I^z \\ \dot{\varphi} \\ \dot{\theta} \\ \dot{\psi} \\ x_I \\ y_I \\ z_I \\ \varphi \\ \theta \\ \psi \\ U_a^1 \\ \Omega_1 \\ U_a^2 \\ \Omega_2 \\ U_a^3 \\ \Omega_3 \end{bmatrix} \tag{35}$$

At the end of the simulation the state information that is returned from *ode45* (i.e. X) is analyzed using *postprocessor.m*. In the postprocessor the data is graphed, and additional information calculated using the state information.

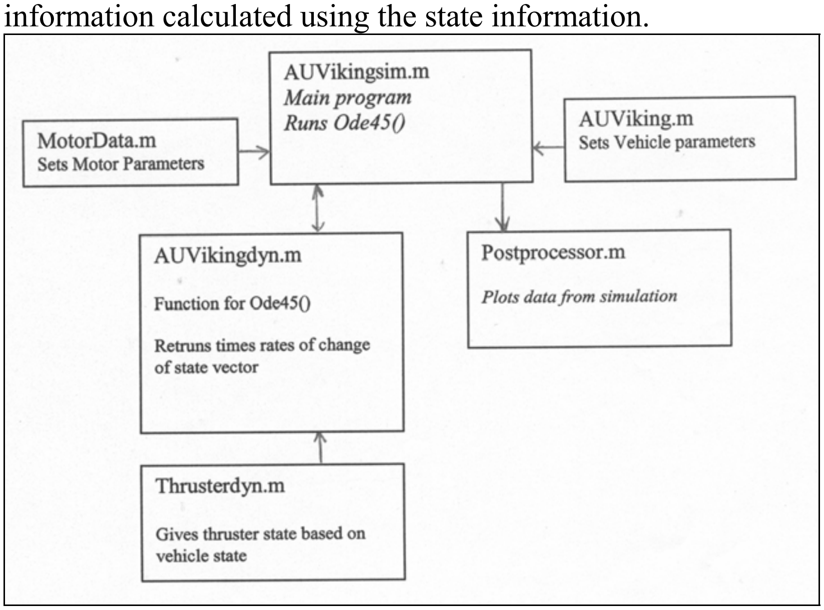

Figure 18 AUViking simulation program architecture

The remainder of this report will look at the results of the numerical analysis for three simple maneuvers. It should be noted that in the simulations discussed below, the initial condition for each quantity in the state vector was zero.

Test Case 1: Dive

The first case that will be examined is a dive. The vertical thruster is ramped up to 12V in 5 seconds. The simulation ran for 30 seconds. In 30 seconds it dives 6 m, and attains a constant velocity of about 0.25 m/s. No motion is seen in the other directions.
Figure 19 shows the power consumption of the thruster as the voltage is ramped up. The first plot in Figure 19 gives the motor power as a function of torque (for reference). At full speed, the motors consume 77 Watts.

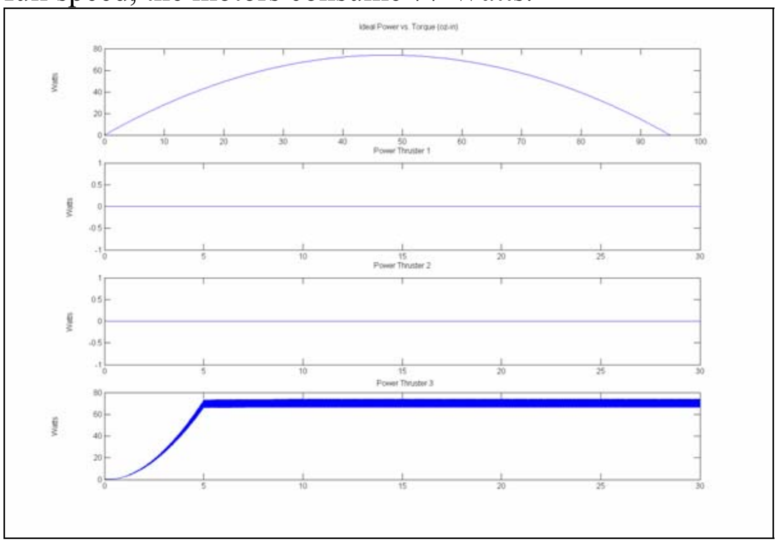

Figure 19 Dive: Power

Figure 20 shows the motor current, torque and rpm. There has been concern about the size of the motors that are going to be used in the thrutsers. The reason that they were going to be used is that they were donated to the team. They have a stall current rating of ~20 amps. Figure 20 shows that the motors are drawing about 14 amps. This means that they are working pretty hard. Max rated load is 5 amps for the motors. This means that these motors may not be sufficient, or they will need to be run at a much lower voltage. The motor data presented here was compared with the typical motor performance curves that are given with the motor (Figure 21) to verify its accuracy. The data shown in Figure 20 and Figure 21 are in strong agreement. The motors could use a reduction gear, or run at a lower voltage to correct this problem.

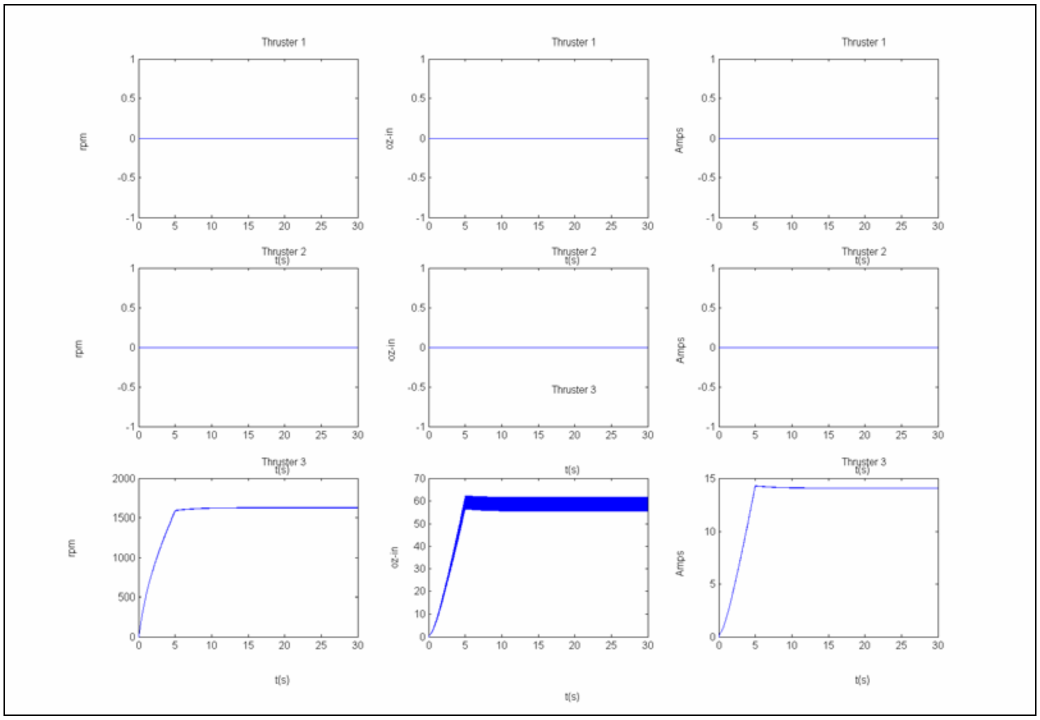

Figure 20 Motor current, torque and rpm

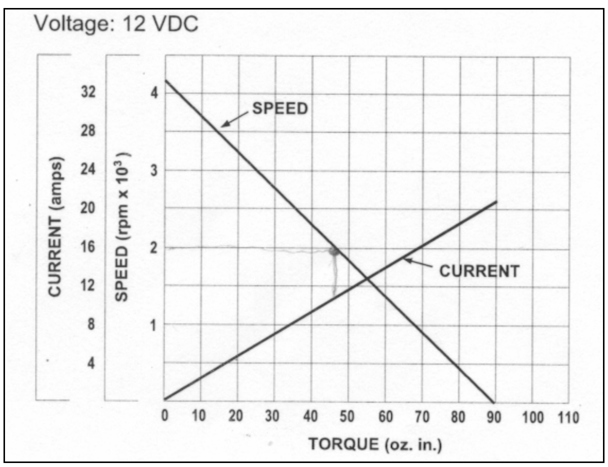

Figure 21 Motor curves given with thruster motors

Test Case 2: Surge

In this test, the two horizontal thrusters are ramped up to 12V in 5s. The simulation was run for 30s. The thrust and the voltage control signals are shown in Figure 22. The thrust shows a brief time lag at the beginning of the test, but then smoothly ascends to a steady state. The smooth transition is what one would expect. The thrust signal shows some noise which is introduced by the numerical approximations. One would expect this in the thrust because it is a "complicated" parameter dependent on a number of state variables. The thrust output is comparable to the results obtained by Healey. The steady state thrust is about 14N for each thruster (~3lbf).

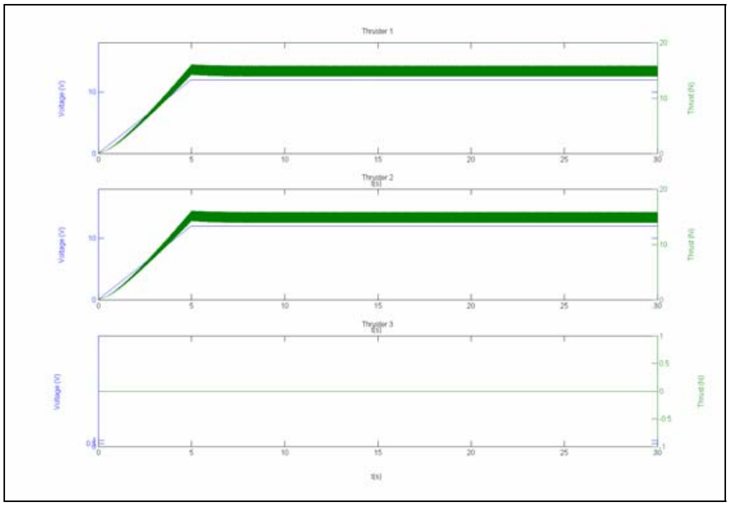

Figure 22 Surge: Thrust and control signal

Figure 23 shows the motion of the vehicle. It reaches a top speed of about .7m/s, and travels 18m in 30 seconds. It can also be seen that vehicle is tending to drive itself upwards slightly as a result of the center of pressure located 1" above the center of gravity on the front of the vehicle. A second simulation was with the center of pressure located 2" above the center of gravity on the front of the vehicle. Figure 24 shows the vehicle motion for the second surge case. It is found that the vehicle rises 1.2 m in the second case, and about 0.6m in the first case. By this rough trial, it is seen that the location of drag center has a significant effect on the results of the simulation.

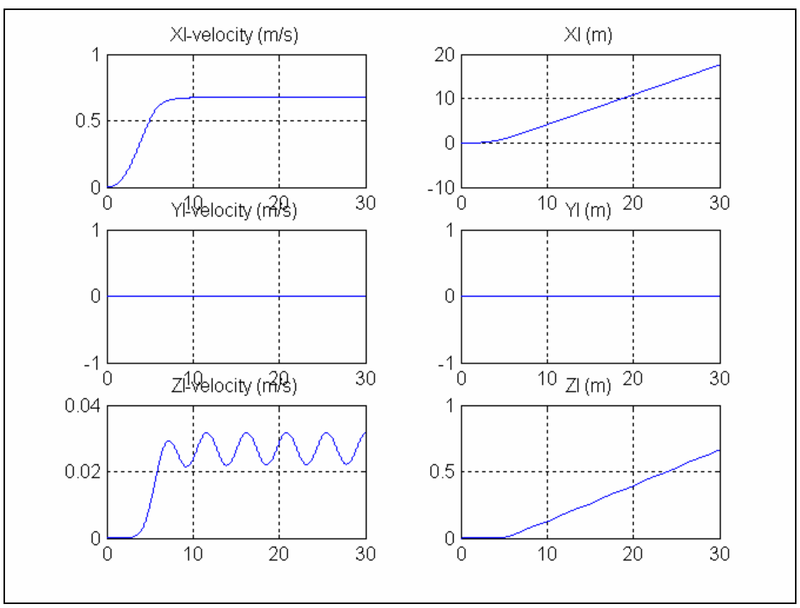

Figure 23 Surge: Vehicle Motion (CP 1" above CG on FP)

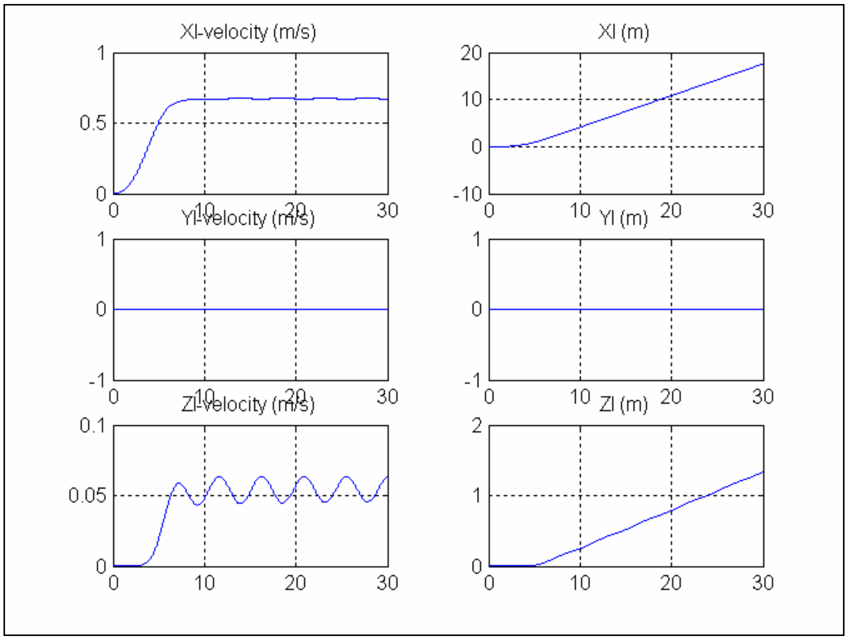

Figure 24 Surge: Vehicle Motion (CP 2" above CG on FP)

Figure 25 shows the vehicle orientation the rates of change in vehicle orientation as a function of time. Oscillations about the y-axis due to the location of the center of pressure on the fore plane are seen in the theta-dot and theta plots. The oscillating nature of the motion is due to the buoyancy force. As the vehicle is disturbed, the buoyancy force stabilizes it.

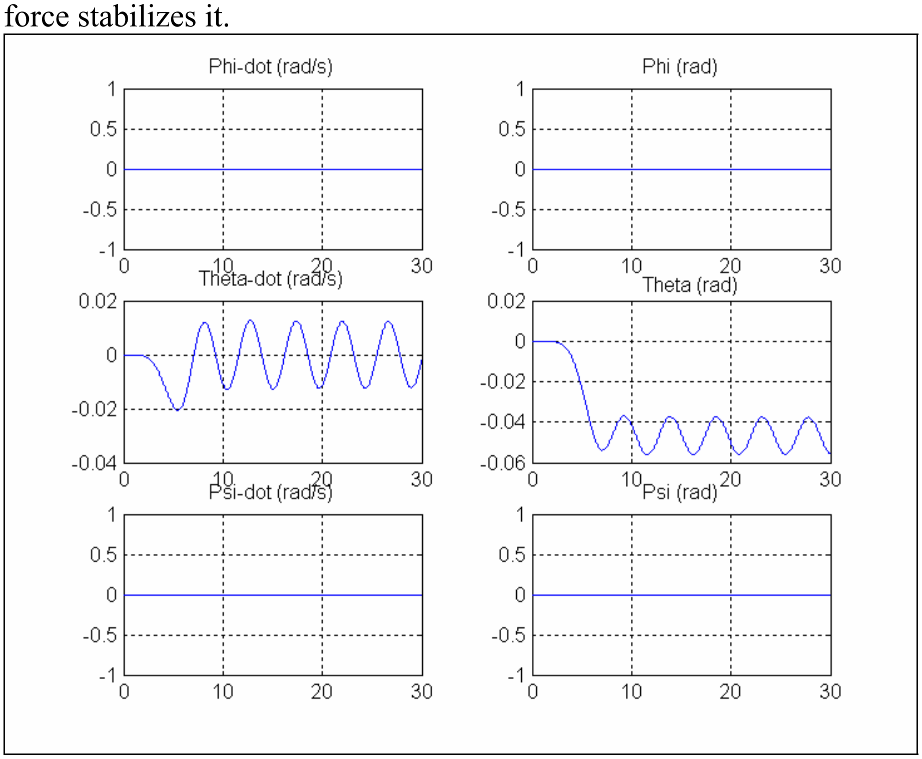

Figure 25 Surge: vehicle orientation

Test Case 3: Turn

The last maneuver that will be considered will be a turn. The port side thruster was turned on to 3V. The simulation was run for 15 seconds. In this time the vehicle reaches a top speed of .1 m/s and makes nearly a full turn (Figure 26). It is also found that the vehicle again begins to pitch and roll slightly (Figure 27). This is again due to the drag force induced moment. Figure 27 shows that the vehicle orientation about the z-axis changes by 2π.

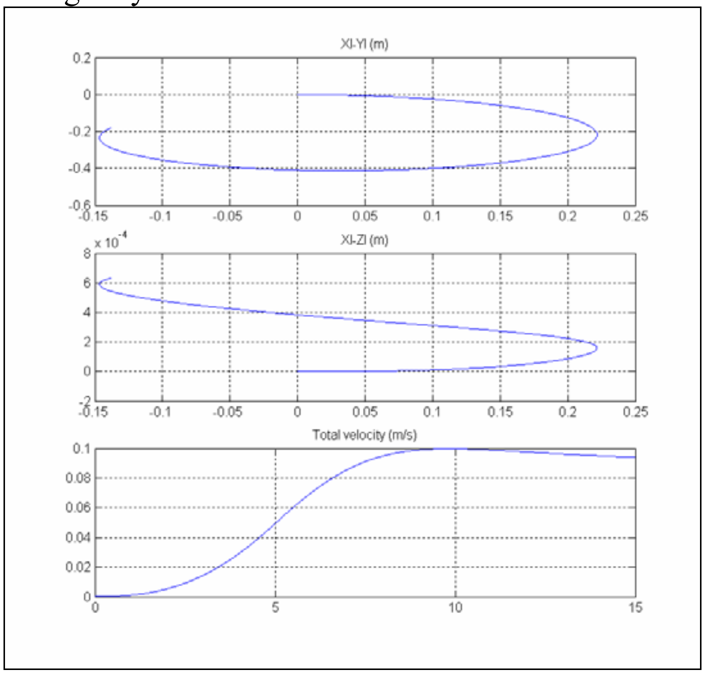

Figure 26 Vehicle path and velocity

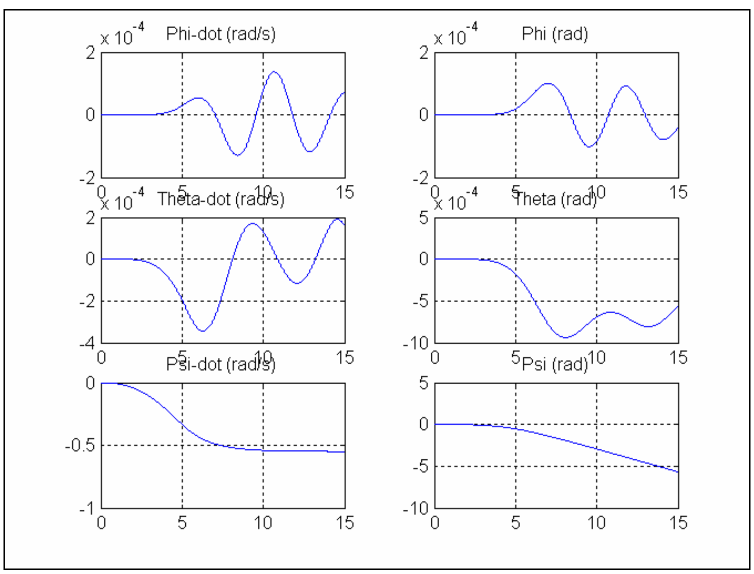

Figure 27 Turn: vehicle orientation

Conclusions

The goal of this project was to develop a numerical model of an AUV that coupled an appropriate thruster model with an approximate underwater vehicle model. The development of this model was meant to promote an understanding of the dynamics of underwater vehicles and create a useful design tool for AUVic. All of these goals were achieved.

In this project, the governing vehicle dynamics were reviewed first. Then, the hydrodynamic forces on the vehicle were considered. For the numerical vehicle model, estimates of the added mass and inertia were found using the strip theory technique. The translational drag of the vehicle was estimated using available empirically determined drag coefficients. Drag coefficients for the rotational motion of the vehicle were estimated using available 2D translational coefficients. Next, Healey's thruster model was reviewed [2]. His four quadrant thruster model combined an armature controlled motor model, a theoretical propeller mapping using airfoil theory, and a fluid momentum model (applied within the finite volume of the shrouded region). Finally, a program that was used to numerically model the ARCS vehicle was modified to represent AUViking. The Healey thruster model was adapted to represent AUViking's thrusters, and estimates of the hydrodynamic forces were incorporated into the numerical model. Several simulations were run. Three simulations were reviewed in this report.

This project produced many insights into the design of the AUViking. Some key ones were:

1. The thruster motors need to be geared down, or powered at a lower voltage
2. The shape of the hull makes the vehicle sensitive to thruster placement
3. The propeller size is sufficient
4. The vehicle speed, given the thruster sizes, will be sufficient

In the future, experimental work could be carried out on AUViking and its thrusters. The results of these experiments could be compared to the numerical model results. Also the effects of positioning drag forces on the pressure centers of the vehicle's front, back and side panels could be explored further.

References

[1] D. Yoerger and J.J.E. Slotine, “Robust trajectory control of underwater vehicles,”IEEE J. Oceanice Eng., vol. OE-10, pp. 462-470, Oct. 1985
[2] J. Healey, S.M. Rock, S. Cody, D. Miles, and J.P. Brown, “Toward an improved understanding of thruster dynamics for underwater vehicles,” IEE J. Oceanic Eng., vol. 20, pp. 354-361, Oct. 1995
[3] J. Craig, Introdution to Robotics, mechanics and control, Addisson Wesley, 1988
[4] Caccia, M., Veruggio, G., “Modeling and Identification of Open-Frame Variable Configuration Unmanned Underwater Vehicles”, IEEE J. Oceanic Eng., vol. 25, no. 2, April 2000
[5] T.I. Fossen, Guidance and Control of Ocean Vehicles. London, U.K.: Wiley, 1994
[6] F. M. White, Fluid Mechanics. Toronto: McGraw Hill, 1999
[7] W.P.A. Van Lammeren, J.D. Van Manen, and M. W. C. Oosterveld, “The Wageningen B-secrew series,” Ttans, SAME, pp. 269-317, Nov. 1969